Multi-slice finite difference method for full potential calculation of low energy electron diffraction spectra

2007 J. Phys.: Condens. Matter 19 386203

(http://iopscience.iop.org/0953-8984/19/38/386203)

IOP PUBLISHING JOURNAL OF PHYSICS: CONDENSED MATTER

J. Phys.: Condens. Matter **19** (2007) 386203 (8pp) doi:10.1088/0953-8984/19/38/386203

Multi-slice finite difference method for full potential calculation of low energy electron diffraction spectra

Huasheng Wu[1], **Jing Wang**[1], **Ricky So**[1] **and S Y Tong**[2]

[1] Physics Department, University of Hong Kong, Hong Kong
[2] Physics Department, City University of Hong Kong, Hong Kong

Received 9 May 2007, in final form 27 June 2007
Published 29 August 2007
Online at stacks.iop.org/JPhysCM/19/386203

Abstract

We propose a multi-slice finite difference method for full potential calculation of low energy electron diffraction spectra. This method keeps the accuracy of the original finite difference (FD) method but reduces the required storage memory and computation time by more than two orders of magnitude. The gain in speed and reduction in memory requirement allow, for the first time, full potential LEED spectra calculations to be carried out for many realistic systems. In this method, the unit cell of a crystal is divided into thin slices in the depth direction. The reflection and transmission coefficients of each slice are calculated by the FD method. The final reflectivity of the crystal is obtained by combining contributions from all slices using a simple recurrent formula.

An understanding of many properties of a solid surface depends on accurate determination of the surface structure. Up to now, most surface structures have been determined by the low energy electron diffraction (LEED) technique. The accuracy of this technique relies on both experimental measurements and theoretical calculations. On the experimental side, the accuracy has improved steadily in recent years, thanks to advances in equipment such as a better-quality LEED screen and higher-resolution CCD camera etc. On the theoretical side, the multiple-scattering (MS) method developed more than three decades ago worked well in many materials. In the MS method, an essential simplification is that the crystal potential around a nucleus is isotropic within a radius and the interstitial potential between atoms is constant. This is the so-called muffin-tin potential [1]. The MS theory succeeded in producing small R-factors [2] compared to experimental LEED spectra in many materials, such as metals, where the atomic potential around each nucleus is indeed quite isotropic. On semiconductor surfaces, however, the MS method usually produced larger R-factors due to stronger anisotropies in the scattering potential due to covalent bonding between atoms.

Over the years, a number of approaches were developed to treat scattering from the full crystal potential [3–8]. The approach with most promise is the finite difference (FD) method proposed by Joly in 2001 [8]. In Joly's calculations, a three-dimensional (3D) uniform orthogonal grid is used to partition a unit cell. The value of the wavefunction is unknown at each

grid point. The Laplacian in the Schrödinger's equation is replaced by a linear combination of wavefunctions at neighboring grid points. In the vicinity of a nucleus, the wavefunction is expanded in radial functions and spherical harmonics. All unknowns can be solved from a system of linear equations. A successful application of this approach was demonstrated in the calculation of x-ray absorption of the near-edge structure. As noted by Joly, this method is too computationally demanding to be practical.

In this paper, we present a multi-slice approach to the FD method. Our method reduces the memory requirement and computation time of the FD approach by more than two orders of magnitude. In our method, the unit cell is divided into thin horizontal slices along the depth direction and the reflection and transmission coefficients of each slice are calculated. The reflectivity of the system is obtained by combining the contributions of all the slices using a simple recurrent formula. As demonstrated in this paper, the gain in speed and reduction in memory requirement allow full potential LEED spectra calculations to be carried out for many realistic systems.

An incoming plane wave with magnitude 1 and wavevector $\vec{k}_0 = \vec{k}_{0\parallel} + \vec{k}_{0\perp}$ is incident from vacuum on a crystal surface and scatters off atomic potentials inside the crystal, $V(\vec{r})$. Part of the wave is reflected along directions with wavevectors $\vec{k}^-_{\vec{g}} = \vec{k}^-_{\vec{g}\parallel} + \vec{k}^-_{\vec{g}\perp}$ and unknown reflection coefficients $A^-_{\vec{g}}$, and part of the wave is transmitted through the crystal slab along directions with wavevectors $\vec{k}^+_{\vec{g}} = \vec{k}^+_{\vec{g}\parallel} + \vec{k}^+_{\vec{g}\perp}$ and unknown transmission coefficients $A^+_{\vec{g}}$. From two-dimensional (2D) momentum conservation, we have $\vec{k}^{+-}_{\vec{g}\parallel} = \vec{k}_{0\parallel} + \vec{g}$, where $\vec{g}$ is a two-dimensional reciprocal lattice vector of the crystalline slab. The reflectivity of beam $\vec{g}$ is calculated as $R_{\vec{g}} = \frac{k^-_{\vec{g}\perp}}{k_{0\perp}} |A^-_{\vec{g}}|^2$.

To find $A^+_{\vec{g}}$ and $A^-_{\vec{g}}$, uniform grids are constructed for each unit cell with step sizes h_x, h_y, h_z along the three orthogonal axes. There is a matching plane near the top and another near the bottom, respectively, of the crystal slab. At a grid point i, between (including) the two matching planes, the wavefunction φ_i satisfies the Schrödinger's equation: $-\frac{\hbar^2}{2m}(\frac{\partial^2}{\partial x^2} + \frac{\partial^2}{\partial y^2} + \frac{\partial^2}{\partial z^2})\varphi_i + (V_i + \mathrm{j}V' - E)\varphi_i = 0$, where V_i and V' are respectively the real and imaginary potentials and E is the electron energy. To do the calculation, each second-order derivative is replaced by a fourth-order finite difference, for example,

$$\frac{\partial^2}{\partial z^2}\varphi(x, y, z) = \frac{1}{h_z^2}\left[\frac{4}{3}(\varphi(z + h_z) + \varphi(z - h_z)) - \frac{1}{12}(\varphi(z + 2h_z) + \varphi(z - 2h_z)) - \frac{5}{2}\varphi(x, y, z)\right]. \quad (1)$$

At points above the upper matching plane, the wavefunction is expressed in terms of the incident and reflected plane waves:

$$\varphi(\vec{\rho}, z) = \mathrm{e}^{\mathrm{j}\vec{k}_{0\parallel}\cdot\vec{\rho}}\mathrm{e}^{\mathrm{j}k_{0\perp}z} + \sum_{\vec{g}} A^-_{\vec{q}}\mathrm{e}^{\mathrm{j}(\vec{k}_{0\parallel}+\vec{g})\cdot\vec{\rho}}\mathrm{e}^{-\mathrm{j}k^-_{\vec{g}\perp}z} \quad (2)$$

where $\vec{\rho}$ is a 2D surface vector. Similarly, at points below the lower matching plane, the wavefunction is expressed in terms of transmitted plane waves:

$$\varphi(\vec{\rho}, z) = \sum_{\vec{g}} A^+_{\vec{g}}\mathrm{e}^{\mathrm{j}(\vec{k}_{0\parallel}+\vec{g})\cdot\vec{\rho}}\mathrm{e}^{\mathrm{j}k^+_{\vec{g}\perp}z}. \quad (3)$$

Surrounding each nucleus, we construct a cubic boundary about 0.3–0.5 Å from the nucleus. At points inside the cube, the wavefunction is expanded in spherical functions:

$$\varphi(r, \vartheta, \phi) = \sum_{lm} A_{lm} R_l(r) Y_{lm}(\vartheta, \phi) \quad (4)$$

where (r, ϑ, ϕ) are the spherical coordinates of a point with respect to the nucleus. The radial function $R_l(r)$ satisfies the usual one-dimensional (1D) differential equation [9].

On the four sides of the unit cell, wavefunctions satisfy periodic boundary conditions. On the upper matching plane, the lower matching plane and the cubic boundary, the boundary conditions are obtained by multiplying a complex conjugate of the corresponding eigenfunction and summing over points on the corresponding boundary as

$$\sum_{\vec{\rho}} \varphi(\vec{\rho}, z) \mathrm{e}^{-\mathrm{j}(\vec{k}_{0\parallel}+\vec{g}')\cdot\vec{\rho}} = [\mathrm{e}^{\mathrm{j}k_{0\perp}z}\delta_{\vec{g}',0} + A^{-}_{\vec{g}'}\mathrm{e}^{-\mathrm{j}k^{-}_{\vec{g}'\perp}z}]N_{\mathrm{s}} \tag{5}$$

$$\sum_{\vec{\rho}} \varphi(\vec{\rho}, z) \mathrm{e}^{-\mathrm{j}(\vec{k}_{0\parallel}+\vec{g}')\cdot\vec{\rho}} = A^{+}_{\vec{g}'}\mathrm{e}^{\mathrm{j}k^{+}_{\vec{g}'\perp}z}N_{\mathrm{s}} \tag{6}$$

$$\sum_{i} \varphi(r_i\vartheta_i\phi_i) Y^{*}_{l'm'}(\vartheta_i\phi_i) = \sum_{lm} A_{lm} \left\{ \sum_{i} R_l(r_i) Y_{lm}(\vartheta_i\phi_i) Y^{*}_{l'm'}(\vartheta_i\phi_i) \right\} \tag{7}$$

where N_{s} is the number of surface grid points, $\vec{g}'$ has $N_{\vec{g}}$ values and $l'm'$ have N_{lm} values.

All unknowns, the wavefunctions at grid points, φ_i, the reflection and transmission coefficients, $A^{-}_{\vec{g}}$ and $A^{+}_{\vec{g}}$, and the expansion coefficients, A_{lm}, are coupled in a system of equations as $AX = B$. Since the majority matrix elements come from formula (1), which describes the relation among the nearest-and second-nearest-neighbor points, the system matrix A is sparse and banded. Under our arrangement, the first and the last $N_{\vec{g}}$ rows in A contain the coefficients appearing in equations (5) and (6), respectively. The matrix B has a single column, with the only non-zero elements being the one element from the first term on the right-hand side of equation (5) and the 2*Ns elements from the first term on the right-hand side of equation (2). Under this arrangement, the reflection and transmission coefficients, $A^{-}_{\vec{g}}$ and $A^{+}_{\vec{g}}$, are the first and last $N_{\vec{g}}$ elements in the single column matrix X.

The number of non-zero elements in matrix A can be estimated as follows. There are three parts involved: the bulk grids (formula (1)), the surfaces (formula (2), (3), (5), (6)) and the vicinity of nuclei (formula (4), (7)). Without symmetry consideration, the number of non-zero elements from the bulk grids is $N_1 = N_{\mathrm{M}}N_{\mathrm{v}}N_{\mathrm{h}}n_i$, where N_{M} is the number of mesh points in a volume occupied by one atom, N_{v}, N_{h} are the number of atoms per unit cell in the vertical and horizontal directions respectively, and n_i is the number of neighboring grid points needed for implementing the Laplacian at a grid point. $N_{\mathrm{M}} = (a/h)^3$, where a is the side length of the volume occupied by one atom, and h is the step size of the grid. An acceptable step size is $1/6$ of the electron wavelength λ, e.g. $h = \lambda/6 = (2\pi/k)/6 \approx 1/k$. So, $N_1 = (ak)^3 N_{\mathrm{v}}N_{\mathrm{h}}n_i$. When symmetry is considered, the number of grid points and hence N_1 will be reduced by a factor of S, the number of symmetry operations. Without symmetry considerations, the number of non-zero elements from the two surfaces is $N_2 = 2N_{\mathrm{s}}N_g$, with N_{s} being the number of surface grid points and N_g the number of reflection or transmission beams. $N_{\mathrm{s}} = (a/h)^2 N_{\mathrm{h}}$, and $N_g = \pi n_k^2$, with n_k being the number of beams along one dimension. $n_k = (k/g) = k/(2\pi/an_1)$, where g is the basic reciprocal vector length and n_1 is the number of atoms along one surface direction. Put together, $N_2 = (ak)^4 N_{\mathrm{h}}^2/2\pi$, where we have put $n_1^2 = N_{\mathrm{h}}$. With symmetry considerations, both the number of surface grid points and the number of beams will be reduced by a factor of S. So N_2 will be reduced by a factor of S^2. Compared to the bulk and surface parts, the part in the vicinity of nuclei is much smaller. Therefore the total number of non-zero elements in A is about

$$M \sim n_i(ak)^3 N_{\mathrm{v}}N_{\mathrm{h}}/S + (ak)^4 (N_{\mathrm{h}}/S)^2/2\pi. \tag{8}$$

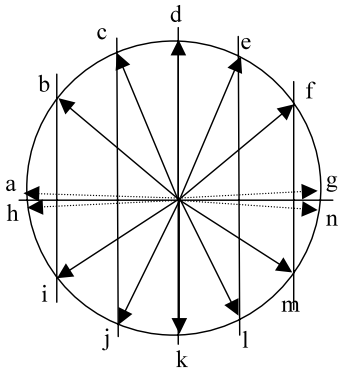

Figure 1. Allowed reflection and transmitting beams of a crystal slab for normal incidence. Beams with dashed lines represent evanescent beams.

For a small unit cell with orthogonal basic vectors and without taking into account any symmetry considerations, $n_i = 13$, $N_v \geqslant 15$, $N_h = 1$, $S = 1$, and $ak \sim 20$. Then the number of non-zero elements, M, is dominated by the first term in formula (8) and $M \sim 1.6 \times 10^6$. Such a number is too large for practical calculations.

To speed up the calculation, we introduce a multi-slice approach. The unit cell is divided into thin horizontal slices. The thickness of each slice is chosen to be as thin as possible, with the limit that the entire cube around a nucleus is contained in the same slice. For the (111) surface of the diamond structure, for example, some slices may contain two layers of atoms ($N_v = 2$) but other slices may not contain any atoms ($N_v = 0$) at all, leading to an average $N_v = 1$. In this way, the number of non-zero elements in matrix A can be reduced by a factor of $N_v \geqslant 15$.

In the case of normal incidence from vacuum, the allowed beams on a typical slice are shown schematically in figure 1, with the dashed lines representing evanescent beams. Take any one of the beams as the incident beam, one will have the same beams as outgoing beams. Writing the reflection coefficients from above and below as r^- and r^+, and the transmission coefficients from below and above as t^- and t^+, and using the notation $\{i_1 i_2 \ldots i_{M-1} i_M; j_1 j_{2\ldots} j_{M-1} j_M\}$ to represent $M \times M$ matrices, with the first M indices representing rows and the last M indices representing columns, we can write, for the case shown in figure 1 where there are seven upward and downward beams, the four matrices of the slice as

$$\begin{aligned} r_l^- &= \{hijklmn; abcdefg\}; \qquad r_l^+ = \{abcdefg; hijklmn\}; \\ t_l^+ &= \{hijklmn; hijklmn\}; \qquad t_l^- = \{abcdefg; abcdefg\} \qquad (l = 1, 2, \ldots N). \end{aligned} \tag{9}$$

The elements of the matrices shown in (9) can be generated using the system matrix A and a multi-column matrix B, where each column corresponds to an allowed incoming beam. For downward incoming beams, the top and bottom $N_{\vec{g}}$ elements in the corresponding column of the solution matrix X are r^- and t^+ respectively. For upward incoming beams, the top and bottom $N_{\vec{g}}$ elements in X are t^- and r^+, respectively.

To combine the slices together, we define R_{l+1}^- as the combined upward reflection coefficient matrix for the total contribution from the deepest slice N up to slice $l + 1$. When slice l is added, the coupling is shown in figure 2, where the new combined reflection coefficient matrix is

$$R_l^- = r_l^- + t_l^+ R_{l+1}^- [I - r_l^+ R_{l+1}^-]^{-1} t_l^- \qquad (l = N - 1, N - 2, \ldots, 3, 2, 1). \tag{10}$$

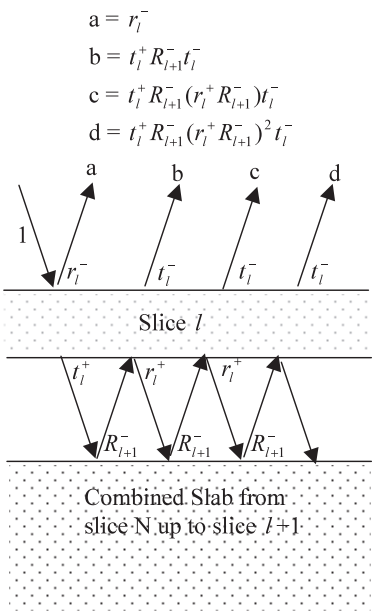

Figure 2. Combining slice l with slab of $l + 1$ to N slices.

In (10), I is an identity matrix and the exponent '-1' denotes matrix inversion. Formula (10) has included all internal reflections between slice l and the slab below it. The stacking procedure starts from the deepest slice, N, where $R_N^- = r_N^-$, and when slice $N - 1$ is placed on it, formula (10) is used to calculate R_{N-1}^-. This procedure is continued until the top slice, $N = 1$, is added and we obtain the total reflection coefficient $R_1^- = \{hijklmn; abcdefg\}$. The beam-wise final reflection coefficients, in the case shown in figure 1 where beam k is the incident beam from vacuum, are the elements located on row k in the matrix R_1^-.

This coupling method is similar to the layer-doubling method for multiple-scattering LEED [9] in that both methods combine reflection and transmission amplitudes from multiple slices. There are two differences. First, the layer-doubling method usually combines together two slices with the same thickness, while this method combines slices with arbitrary thickness. Second, in the layer-doubling method, each small slice should contain at least one layer of atoms, while in this method each slice does not need to have any atoms ($N_v = 0$) so that the thickness of each slice can be very small.

For a large unit cell, the number of atoms in the horizontal plane, n_h, is large. As a result, the non-zero elements in the second term of equation (8) will dominate. For efficient calculation, the use of full symmetry of a system is essential, which can reduce the second term in formula (8) by a factor of S^2, where for normal incidence, $S = 4$ for the (110) surface, $S = 6$ for the (111) surface and $S = 8$ for the (100) surface. For an off-normal incident beam, for example beam f in figure 1, the symmetry of the system is lowered. However, we obtain savings by considering the effect of beam f together with its equivalent beam, j, on the slice. As a result, instead of calculating reflection and transmission coefficients expressed in formula (9), we calculate the rearranged reflection coefficient matrix as $r_l^- = \{h + n, i + mj + lk; abcd\}$ and other similar ones. The implementation of this rearrangement simply adds together columns h and n, columns i and m, and columns j and l, in the matrix B mentioned earlier.

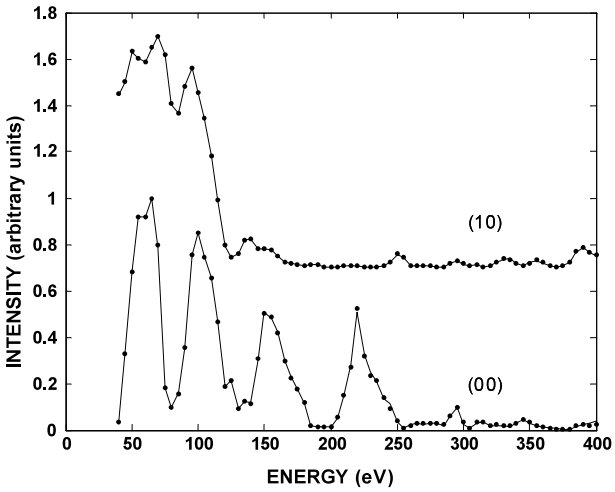

Figure 3. IV curves for diamond (111), the 1×1 surface. Solid lines are calculated by the FD method using a thick slab and the diamonds are results of the MSFD method.

For the (111) surface of a diamond structure, the basis vectors are non-orthogonal. To implement the Laplacian in Schrödinger's equation, we need to write:

$$\left(\frac{\partial^2}{\partial x^2} + \frac{\partial^2}{\partial y^2}\right)\varphi = \frac{2}{3}\left(\frac{\partial^2}{\partial a^2} + \frac{\partial^2}{\partial b^2} + \frac{\partial^2}{\partial c^2}\right)\varphi \tag{11}$$

where a, b, c are the three symmetry directions of the (111) surface and each of the three second-order derivatives on the right-hand side of formula (11) is calculated using formula (1). The total number of points, n_i, for implementing the Laplacian increases slightly from 13 to 17, while keeping the same accuracy.

In calculation, the criterion for truncating expansions in formula (2)–(7) is that the absolute values of A_g^+, A_g^- at large g and A_{lm} at large l, m are smaller than 0.1% of the largest corresponding values.

To demonstrate the accuracy of the multi-slice finite difference method, we show in figure 3 the IV curves of diamond (111), the 1×1 surface. The solid lines are calculated using a very thick crystal slab, while the dots are results obtained from the multi-slice finite difference method, using one atom per slice on average. Clearly, the two calculations produce essentially the same IV curves. In this calculation, 61 g values (beams) are used (including evanescent beams). The truncating value of l is 10, which corresponds to 100 A_{lm}.

In figure 4, we show the results of six beams for a relaxed Si(111) 1×1 surface, comparing experiment [10] (top curve) and different computation methods. The fourth curve in each panel is calculated using the new multi-slice finite difference (MSFD) method with a full potential (FP). We have used the full potential generated by an *ab initio* total energy calculation program called Wien2k [11]. The third curve is calculated using our MSFD method, where we have used a muffin-tin averaged potential (MTP) of the full potential. The second curve is calculated using the conventional multiple scattering (MS) LEED program [12] using eight phase shifts generated from the same muffin-tin potential used for the third curve. The optimal atomic positions are determined by best fit with the experiment using the conventional MS method [10]. Comparing the second and third sets of curves, we see that our MSFD results and the conventional MS method results using the same muffin-tin potential produced similar IV curves, for strong as well as weak features. The remaining differences are numerical and undetectable by

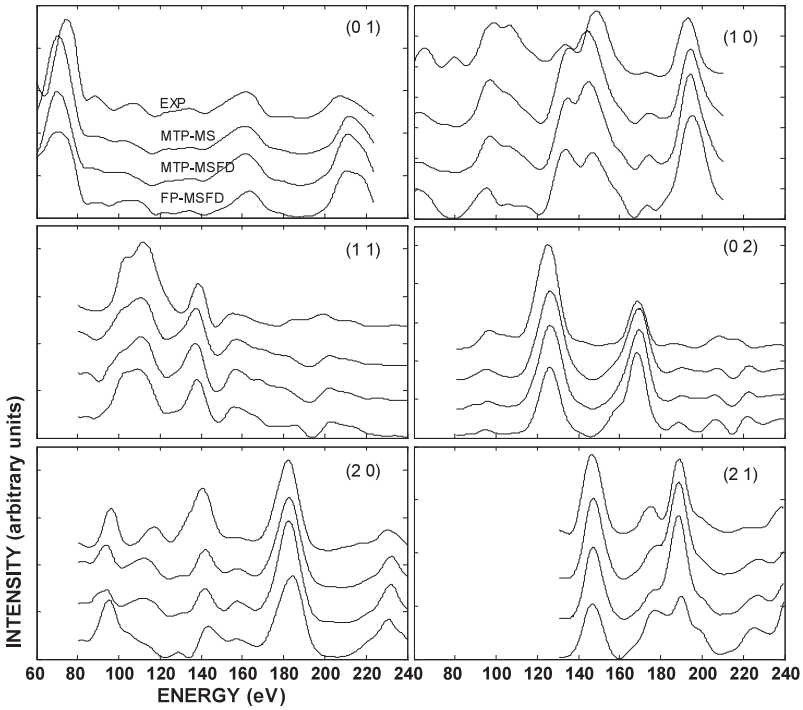

Figure 4. *I V* curves for Si(111), the 1×1 surface. In each panel, the top curve is from experiment. The fourth curve is calculated by our MSFD method with full potential (FP). The third curve is calculated by the MSFD method using a muffin-tin potential (MTP) derived from the full potential. The second curve is calculated by the conventional MS method using eight phase shifts from the same MTP as for the third curve.

eye. We attribute the numerical differences to minor variations in the two computation schemes. These include using only real potential phase shifts (an inconsistency in the MS method) and the neglect of internal reflections at the vacuum–solid interface for the MS method. In our MSFD method, the optical potential (with inelastic damping) is used throughout and the wavefunctions are properly matched at the vacuum–solid interface. Of more interest is that our MSFD calculations using the full potential resulted in appreciable differences from that using the muffin-tin potential, especially for the weaker beams. For the MSFD calculations, the grid size used is around 0.1 Å and it takes 700 M bytes of memory and 50 s for each energy point.

We have also calculated larger unit cell systems using the MSFD method. For a Si(111) 2×2 surface and a C(111) 3×3 surface, the calculations require about 3 Gigabytes of memory and 20 min for each energy point. It is anticipated that, with today's parallel computers, it will be practical to use our full potential MSFD method to calculate even larger systems of interest.

Acknowledgment

This work is supported by Hong Kong Research Grants Council grant no. HKU704605.

References

[1] Tong S Y 1999 *Adv. Phys.* **48** 135
[2] Pendry J B 1980 *J. Phys. C: Solid State Phys.* **13** 937–44

[3] Joly Y 1992 *Phys. Rev. Lett.* **68** 950
[4] Huhne T, Zecha C, Ebert H, Dederichs P H and Zeller R 1998 *Phys. Rev.* B **58** 10236
[5] Ahlers D, Schutz G, Popescu V and Ebert H 1998 *J. Appl. Phys.* **83** 7082
[6] Ahlers D, Attenkofer K and Schutz G 1998 *J. Appl. Phys.* **83** 7085
[7] Huhne T and Ebert H 1999 *Solid State Commun.* **109** 577
[8] Joly Y 2001 *Phys. Rev.* B **63** 125120
[9] Tong S Y 1975 *Prog. Surf. Sci.* **7** 1–48
[10] Jona F, Marcus P M, Davis H L and Noonan J R 1986 *Phys. Rev.* B **33** 4005
[11] Blaha P, Schwarz K, Madsen G, Kvasnicka D and Luitz J Inst. f. Materials Chemistry, TU Vienna
[12] Van Hove M A, Moritz W, Over H, Rous P J, Wander A, Barbieri A, Materer N, Stark U and Somorjai G A 1993 *Surf. Sci. Rep.* **19** 191